

Compressing MIMO Channel Submatrices with Tucker Decomposition: Enabling Efficient Storage and Reducing SINR Computation Overhead

Yuanwei Zhang¹, Ya-Nan Zhu¹ and Xiaoqun Zhang^{2,*}

¹ School of Mathematical Sciences, Shanghai Jiao Tong University, Shanghai 200240, P.R. China.

² School of Mathematical Sciences, MOE-LSC, Institute of Natural Sciences, Shanghai Jiao Tong University, Shanghai 200240, P.R. China.

Abstract. Massive multiple-input multiple-output (MIMO) systems employ a large number of antennas to achieve gains in capacity, spectral efficiency, and energy efficiency. However, the large antenna array also incurs substantial storage and computational costs. This paper proposes a novel data compression framework for massive MIMO channel matrices based on tensor Tucker decomposition. To address the substantial storage and computational burdens of massive MIMO systems, we formulate the high-dimensional channel matrices as tensors and propose a novel groupwise Tucker decomposition model. This model efficiently compresses the tensorial channel representations while reducing SINR estimation overhead. We develop an alternating update algorithm and HOSVD-based initialization to compute the core tensors and factor matrices. Extensive simulations demonstrate significant channel storage savings with minimal SINR approximation errors. By exploiting tensor techniques, our approach balances channel compression against SINR computation complexity, providing an efficient means to simultaneously address the storage and computational challenges of massive MIMO.

1 Introduction

Multiple-input and multiple-output (MIMO) technology utilizes multiple transmission and receiving antennas to exploit multipath propagation [1,2]. It has served as the foundation for wireless and mobile networks such as the fourth (4G) and fifth (5G) generations [3–5]. Compared with MIMO system, massive MIMO significantly improve the spectral and transmit power efficiency by equipping hundreds or even thousands of antennas for base station (BS). With a large number of antennas, BSs in massive MIMO system can serve multiples users simultaneously at very low signal-to-interference noise

*Corresponding author. *Email address:* xqzhang@sjtu.edu.cn (Xiaoqun Zhang)

level [6–8]. For instance, with a sufficiently large number of antennas, linear precoding methods can achieve performance comparable to that of optimal nonlinear schemes [9]. Moreover, if the number of BS antennas tends to be infinity, the impact of noise and intra-interference will vanish [9]. However, the integration of a large number of antennas in a massive MIMO system also presents unprecedented challenges, particularly in terms of computation and storage.

High computational cost is incurred by signal transmission operations involving large channel matrices. Particularly, numerous operations require computational complexity with a cubic dependence on the channel size [10–12]. For example, in this paper we consider the linear minimum mean squared error (MMSE) equalization and singular value decomposition (SVD) precoding method, for achieving an optimal Signal-to-Interference Noise Ratio (SINR) among all linear schemes [13]. This equalization method involves matrix-matrix multiplication and matrix inversion while the precoding method relies on SVD of channel matrices. These operations impose a substantial computational cost on massive MIMO implementations due to the large number of antennas and served users. On the other hand, channel state information (CSI) matrices are necessary for both precoding and equalization. As the number of antennas is significantly larger in massive MIMO than that in traditional MIMO systems, the CSI matrices are considerably larger. As a result, the massive MIMO system requires much higher memory capacity than conventional MIMO systems, often exceeding the size by over 100 times in practical scenarios [14].

Current research usually treats data compression and computational complexity reduction as two distinct objectives. Numerous studies focused on developing efficient and low-complexity algorithms for precoding/equalization. In [15–17], truncation techniques were employed to approximate matrix inversion using a Taylor series expansion for achieving complexity reduction. [18] relies on the low-rankness or sparse properties inherent from the system to effectively reduce complexity. Regarding data compression methods, approaches in [19, 20] focused on reducing the size of channel data by converting it into sparse matrices. [21] employs dimensional reduction or compressive sensing techniques for further compression. [22] introduces a technique that entails grouping analogous channel data from antennas and substituting them with average values and representative group patterns.

In this paper, we consider the orthogonal frequency-division multiplexing (OFDM) based massive MIMO systems. Within each channel, the presence of both line-of-sight (LOS) and none-line-of-sight (NLOS) radio waves can be represented as channel submatrices that contribute to channel matrix through linear combinations [10, 23]. Thus the submatrices within each channel naturally form a 3-order tensor. Research on different tensor decomposition forms has a long history and is continuously evolving. Two well-known tensor decompositions are CANDECOMP/PARAFAC (CP) decomposition [24, 25] and Tucker decomposition [26]. CP decomposition represents a high-order tensor as a sum of rank-one tensors, while Tucker decomposition can be seen as a higher-order extension of principal component analysis (PCA) [27, 28]. Another notable decomposi-

tion is the Tensor-Train decomposition, which has gained popularity in machine learning due to its efficient implementation of basic operations [29,30]. In the context of our problem, since signal processing and SINR calculation predominantly entail matrix product operations, we consider Tucker decomposition to be the most suitable approach for the following signal processing task, considering the benefits of reduced computational complexity when using the compressed data.

We design a Tucker decomposition based model for compressing the channel submatrices in the MIMO system. The outcome of the factorized form can not only reduce the storage cost but also reduce the computational cost of precoding, equalizer and SINR. Through numerical experiments, we demonstrate that our proposed model can achieve significant speedup of factor 6.19 and compression ratio of 6.16, respectively, while maintaining an acceptable level of compressed error around 10%. These results show the potential benefits and feasibility of our approach in practical MIMO system design.

To the best of our knowledge, this paper is the first work that tackle the compression problem of the channel submatrices to reduce both computation and memory cost. The advantages of our compression model can be summarized as follows: The compressed data structure enables direct calculation of the precoder, equalizer, and SINR without reconstructing the channel matrix. This provides significant computational savings, making real-time performance feasible on devices with limited capabilities. Concurrently, compression results demonstrate substantially reduced storage requirements for channel data, enabling feasible storage on devices with constrained capacity.

The remaining sections of this paper are organized as follows. In Section 2, we provide an introduction to the multi-cell multi-user massive MIMO system, highlighting the two main challenges addressed in this paper. We also introduce the tensor notations and explain how the Tucker decomposition method is utilized for compression. The main results of this study are presented in Section 3. Firstly, we introduce a simple compression model based on Tucker decomposition and discuss the key ideas for achieving faster computations. Then, we propose the Groupwise Tucker compression model and present the corresponding algorithms for compressing channel data in Section 3.2. Additionally, we provide a detailed analysis of the reduction in computation complexity of SINR in Section 3.3. In Section 4, we present the numerical results obtained from various experiments conducted to evaluate the performance of the proposed models. Finally, we conclude the paper in Section 5, summarizing the key findings and discussing the implications of our work.

2 Background

In this section, we first present some related notations and introduce the background for MIMO system.

2.1 Notations

- Matrices are denoted by bold capital letters (e.g., \mathbf{H}), vectors are denoted by bold lowercase letters (e.g., \mathbf{x}) and tensors are denoted by bold calligraphic letters (e.g., \mathcal{X}). The index set $[N]$ denotes the set $\{1, 2, \dots, N\}$, where N is a positive integer. $\sqrt{-1}$ represents the imaginary unit.
- \mathbf{A}^* represents the hermitian matrix of \mathbf{A} . $[\mathbf{A}]_r$ represents the r -th column of matrix \mathbf{A} and $[\mathbf{A}]_{1:r}$ represents the first r columns of \mathbf{A} . \mathbf{I}_N denotes the identity matrix with size $N \times N$.
- The bold symbols $\mathbf{H}_k^{[i,j]} \in \mathbb{C}^{M \times N}$ and $\mathcal{X}_k^{[i,j]} \in \mathbb{C}^{M \times N \times P}$ represent the channel matrix and tensor composed of channel submatrices, respectively. In this context, M and N refer to the number of antennas for the receiver and transmitter, respectively, while P represents the number of submatrices. The indices $[i, j]$ correspond to specific users and k serves as the index for the base station. Similarly, we have $\tilde{\mathbf{H}}_k^{[i,j]} \in \mathbb{C}^{m \times n}$ and $\mathcal{G}_k^{[i,j]} \in \mathbb{C}^{m \times n \times p}$, which represent the compressed channel matrix and channel tensor ($m \leq M, n \leq N, p \leq P$).

2.2 Signal Transmission and SINR

As depicted in Figure 1, we consider a general multi-cell multi-user MIMO system, comprising J Base Stations (BSs), with one BS allocated per cell. Let K_i be the number of scheduled users for i th-BS. Each link consists of a BS equipped with N transmit antennas and a user equipment (UE) equipped with M receive antennas. Here, we denote the $M \times N$ channel matrix from k -th BS to j -th UE in i -th cell as $\mathbf{H}_k^{[i,j]}$, $i, k \in [J]$ and $j \in [K_i]$.

For universality, we consider both intra-cell and inter-cell interference. Intra-cell interference occurs when multiple UEs are concurrently scheduled using spatial division technique within the same cell, while the inter-cell interference arises from BSs in neighboring cells when they serve their UEs. Let L denote the spatial streams number, then the received signal $\mathbf{y}^{[i,j]}$ for j -th UE in i -th cell can be expressed as the sum of four distinct components:

$$\mathbf{y}^{[i,j]} = \underbrace{\mathbf{H}_i^{[i,j]} \mathbf{P}^{[i,j]} \mathbf{x}^{[i,j]}}_{\text{desired signal}} + \underbrace{\sum_{l=1, l \neq i}^{K_i} \mathbf{H}_i^{[i,j]} \mathbf{P}^{[i,l]} \mathbf{x}^{[i,l]}}_{\text{intra-cell interference}} + \underbrace{\sum_{k=1, k \neq i}^J \sum_{l=1}^{K_k} \mathbf{H}_k^{[i,j]} \mathbf{P}^{[k,l]} \mathbf{x}^{[k,l]}}_{\text{inter-cell interference}} + \underbrace{\mathbf{z}^{[i,j]}}_{\text{noise}} \quad (2.1)$$

where $\mathbf{P}^{[i,j]}$ is the $N \times L$ precoding matrix and $\mathbf{x}^{[i,j]}$ is the $L \times 1$ transmit-signal vector for j -th UE in i -th cell. $\mathbf{z}^{[i,j]}$ is the additive white Gaussian noise.

For each $\mathbf{H}_k^{[i,j]}$, $i, k \in [J]$ and $j \in [K_i]$, the channel matrix is generated from submatrices with different time-delay. Denote the channel matrix with time-varying as $\mathbf{H}(t)$, then

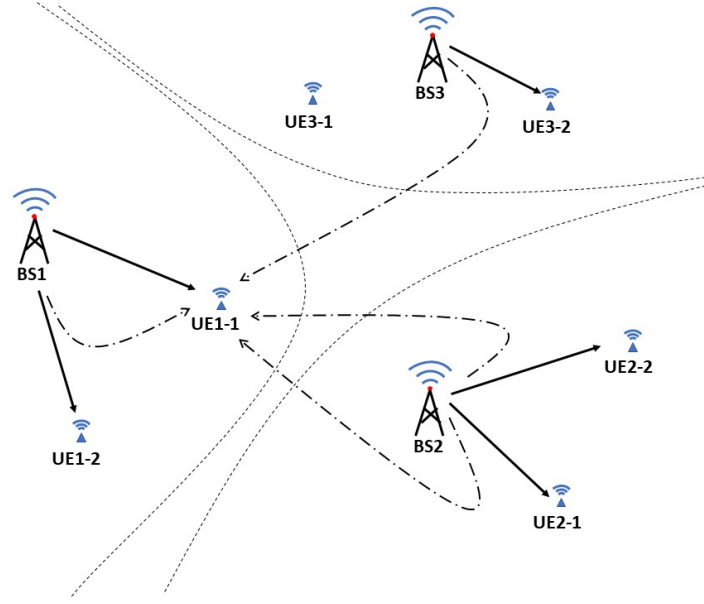


Figure 1: Illustration of a MIMO system. In this MIMO system, each cellular network cell is equipped with a single base station serving two users. The solid lines denote the desired signal paths and the dashed lines signify interference. Specifically, UE1-1 receives the desired signal from BS1, experiencing both intra-cell interference from BS1 and co-channel interference from BS2 and BS3.

$\mathbf{H}(t)$ is comprised of a linear combination of a line-of-sight (LOS) submatrix $\mathbf{H}^{LOS}(t)$ and multiple non-line-of-sight (NLOS) submatrices $\mathbf{H}_l^{NLOS}(t), l=1, \dots, P-1$, as follows:

$$\mathbf{H}(t) = c_0(t-t_0)\mathbf{H}^{LOS}(t_0) + \sum_{l=1}^{P-1} c_l(t-t_0)\mathbf{H}_l^{NLOS}(t_0), \quad (2.2)$$

where P is the number of submatrices and $c_l(t)$ is the time-varying coefficients.

For the receiver, once it has received the signal $\mathbf{y}^{[i,j]}$, the UE utilizes a receive filter matrix $\mathbf{W}^{[i,j]}$ to reconstruct the desired transmit-signal vector $\mathbf{x}^{[i,j]}$, i.e., the estimated desired signal is computed by $\hat{\mathbf{x}}^{[i,j]} = (\mathbf{W}^{[i,j]})^* \mathbf{y}^{[i,j]}$. Here we consider MMSE equalizer [31] and $\mathbf{W}^{[i,j]}$ is defined as follows:

$$\mathbf{W}^{[i,j]} = (\mathbf{Q}^{[i,j]})^{-1} \mathbf{H}_i^{[i,j]} \mathbf{P}^{[i,j]}, \quad (2.3)$$

where $\mathbf{Q}^{[i,j]}$ is the total received signal covariance matrix of j -th UE in i -th cell. Assuming the standard variation of the Gaussian noise as σ , $\mathbf{Q}^{[i,j]}$ can be expressed as:

$$\mathbf{Q}^{[i,j]} = \sum_{k=1}^J \sum_{l=1}^{K_k} \mathbf{H}_k^{[i,j]} \mathbf{P}^{[k,l]} (\mathbf{P}^{[k,l]})^* (\mathbf{H}_k^{[i,j]})^* + \sigma^2 \mathbf{I}_M. \quad (2.4)$$

In accordance with the notations provided above, the SINR of the r -th spatial stream

of j -th UE in i -th cell is calculated as follows:

$$SINR_r^{[i,j]} = \frac{s_r^{[i,j]}}{\left[\mathbf{W}^{[i,j]} \right]_r^* \mathbf{Q}^{[i,j]} \left[\mathbf{W}^{[i,j]} \right]_r - s_r^{[i,j]}} \quad (2.5)$$

where

$$s_r^{[i,j]} = \left| \left[\mathbf{W}^{[i,j]} \right]_r^* \mathbf{H}_i^{[i,j]} \left[\mathbf{P}^{[i,j]} \right]_r \right|^2 \quad (2.6)$$

is the signal power of r -th spatial stream. Here $r \in [L]$ and $[\cdot]_r$ denotes the r -th column vector of the matrix. The denominator represents the power of total interference corresponding to r -th spatial stream.

The equations (2.4) and (2.5) show that the value of SINR depends on the precoding method of transmit signal, receive filter method, and the number of spatial streams, etc. In this paper, we consider the SVD precoding method, which can achieve better channel capacity [32]. Denote $\mathbf{U}^{[i,j]} \mathbf{\Sigma}^{[i,j]} (\mathbf{V}^{[i,j]})^*$ is the truncated- L SVD of $\mathbf{H}_i^{[i,j]}$, where $\mathbf{V}^{[i,j]}$ represents the first L right singular vectors of $\mathbf{V}^{[i,j]}$. Then, the SVD precoding method is given by setting

$$\mathbf{P}^{[i,j]} = \mathbf{V}^{[i,j]}. \quad (2.7)$$

Then the filter matrix $\mathbf{W}^{[i,j]} = (\mathbf{Q}^{[i,j]})^{-1} \mathbf{U}^{[i,j]} \mathbf{\Sigma}^{[i,j]}$ and the signal power, $s_r^{[i,j]} = (\sigma_r^{[i,j]})^4 \left| \left[\mathbf{U}^{[i,j]} \right]_r^* (\mathbf{Q}^{[i,j]})^{-1} \left[\mathbf{U}^{[i,j]} \right]_r \right|^2$, where $\sigma_r^{[i,j]}$ is the r -th singular value. It can be seen that both the calculation of the receive filter $\mathbf{W}^{[i,j]}$ and SINR require intricate operations, including the inversion of the covariance matrix $\mathbf{Q}^{[i,j]}$ and SVD of channel matrices.

These above operations exhibit a substantial level of computational complexity, which becomes even more challenging in the context of uplink signal transmission as the size of the covariance matrix scales with the number of antennas at the base station. This computational challenge becomes particularly undesirable in modern applications like 5G technology, where an increasing number of antennas are utilized to mitigate growing path loss. This, serves as the primary motivation of this paper, aimed at reducing these computational complexities effectively. The second purpose of this paper is to reduce the storage overhead. In practices one need to store the submatrices in (2.2) of all channels at a fix time point for generating the channel matrix. However, those submatrices keeps the same size with channel matrices and have a large number, therefore, it imposes a substantial storage burden, making it impractical, particularly when dealing with an increasing number of users.

2.3 Preliminaries on Tensors

Before proposing the data compression model, we first introduce some notations for tensor based operations and review some related algorithms, readers may refer to [33] for more details.

- *Order of tensor, also known as way or mode*, refers to the number of dimensions. For example, a vector is a 1-order tensor and a matrix is a 2-order tensor.
- *Inner product* of two complex 3-order tensors \mathcal{X} and \mathcal{Y} with the same size is defined by

$$\langle \mathcal{X}, \mathcal{Y} \rangle = \sum_{i_1, i_2, i_3} x_{i_1, i_2, i_3} \bar{y}_{i_1, i_2, i_3}.$$

The induced tensor norm is $\|\mathcal{X}\| = \sqrt{\langle \mathcal{X}, \mathcal{X} \rangle}$.

- *Matricization, or unfolding*, is the reordering of all elements of a tensor into a matrix. For example, the mode-1 matricization of 3-order tensor $\mathcal{X} \in \mathbb{C}^{I_1 \times I_2 \times I_3}$ is denoted as $\mathcal{X}_{(1)} \in \mathbb{C}^{I_1 \times I_2 I_3}$. It is the rearrangement of vectors of length I_1 into a matrix according to the order. More precisely, $[\mathcal{X}_{(1)}]_{i_1, i_2 + n(i_3 - 1)} = \mathcal{X}_{i_1, i_2, i_3}$.
- *Tensor-matrix product*. Denote $\mathcal{X} \times_1 \mathbf{U}$ as the 1-mode product of the tensor $\mathcal{X} \in \mathbb{C}^{I_1 \times I_2 \times I_3}$ with a matrix $\mathbf{U} \in \mathbb{C}^{J \times I_1}$, then $\mathcal{X} \times_1 \mathbf{U} \in \mathbb{C}^{J \times I_2 \times I_3}$. Elementwisely, we have

$$(\mathcal{X} \times_1 \mathbf{U})_{j, i_2, i_3} = \sum_{i_1=1}^{I_1} x_{i_1, i_2, i_3} u_{j, i_1}.$$

It is straightforward to verify that,

$$\mathcal{Y} = \mathcal{X} \times_1 \mathbf{U} \Leftrightarrow \mathcal{Y}_{(1)} = \mathbf{U} \mathcal{X}_{(1)},$$

- *Tucker rank*. Denote $R_n = \text{rank}(\mathcal{X}_{(n)})$, then the vector $\text{rank}_{\text{T}}(\mathcal{X}) = (R_1, R_2, \dots, R_N)$ is the Tucker rank of N -order tensor \mathcal{X} .

With those definitions and operations, We will first introduce the Tucker decomposition method and how directly use Tucker decomposition to compress channel tensors.

- *Tucker decomposition*. Tucker decomposition is a generalization of the PCA method in higher order perspective [26]. For a 3-order tensor $\mathcal{X} \in \mathbb{C}^{I_1 \times I_2 \times I_3}$, it decomposed \mathcal{X} into a smaller tensor \mathcal{G} multiplied three orthogonal factor matrices $\mathbf{A} \in \mathbb{C}^{I_1 \times R_1}, \mathbf{B} \in \mathbb{C}^{I_2 \times R_2}, \mathbf{C} \in \mathbb{C}^{I_3 \times R_3}$ ($I_i \geq R_i, i = 1, 2, 3$), i.e., $\mathcal{X} \approx \mathcal{G} \times_1 \mathbf{A} \times_2 \mathbf{B} \times_3 \mathbf{C}$ through the following optimization problem

$$\begin{aligned} \min_{\mathbf{A}, \mathbf{B}, \mathbf{C}, \mathcal{G}} & \|\mathcal{X} - \mathcal{G} \times_1 \mathbf{A} \times_2 \mathbf{B} \times_3 \mathbf{C}\|_F^2 \\ \text{s.t. } & \mathbf{A}^* \mathbf{A} = \mathbf{I}_{R_1}, \mathbf{B}^* \mathbf{B} = \mathbf{I}_{R_2}, \mathbf{C}^* \mathbf{C} = \mathbf{I}_{R_3} \end{aligned} \quad (2.8)$$

There are two popular algorithms available for solving (2.8): the High Order Singular Value Decomposition (HOSVD) algorithm [34] and the Higher Order Orthogonal Iteration (HOOI) algorithm [35]. The HOSVD algorithm is an extension of

matrix SVD, it leverages the principal left singular vectors from each mode matricization of the target tensor as the factor matrix.

Algorithm 1 HOSVD Algorithm.

Input: Target 3-order tensor $\mathcal{X} \in \mathbb{C}^{I_1 \times I_2 \times I_3}$. The parameters R_1, R_2, R_3 .

- 1: $A \leftarrow R_1$ leading left singular vectors of $\mathcal{X}_{(1)}$.
- 2: $B \leftarrow R_2$ leading left singular vectors of $\mathcal{X}_{(2)}$.
- 3: $C \leftarrow R_3$ leading left singular vectors of $\mathcal{X}_{(3)}$.
- 4: $\mathcal{G} = \mathcal{X} \times_1 A^* \times_2 B^* \times_3 C^*$

Output: Core tensor \mathcal{G} , factor matrices A, B, C .

The solutions obtained from the HOSVD algorithm are usually not optimal solution of (2.8). The HOOI algorithm incorporates the HOSVD algorithm as an initialization method and employs an alternating iteration approach to achieve a more accurate solution [35].

3 Methods

3.1 Channel Matrices in tensor form

Stacking the submatrices $H^{LOS}(t)$ and $H_l^{NLOS}(t), l=1, \dots, P-1$ in (2.2) along with third-mode as a tensor. (2.2) can be reformulated as the following tensor-vector product

$$H(t) = \mathcal{X}(t_0) \times_3 c^*(t - t_0), \quad (3.1)$$

where $c(t) = [c_1(t), c_2(t), \dots, c_P(t)]' \in \mathbb{C}^{P \times 1}$ is the coefficient vector. Denote the tensor for each channel as $\mathcal{X}_k^{[i,j]}$ and we want to apply decomposition method to compress those channel tensors while reduce the SINR estimation overhead,

The key idea in our proposed compression model to reducing computational complexity lies in leveraging the orthogonality of factor matrices within the decomposition form and canceling them out during SINR calculations. As a result, the sizes of matrix involved in the computations correspond to the compressed scale, thereby decreasing computational complexity.

- **Individual Tucker compression.** For each 3-order tensor $\mathcal{X}_k^{[i,j]} \in \mathbb{C}^{M \times N \times P}$. The tucker decomposition find the factor matrices $A_k^{[i,j]} \in \mathbb{C}^{M \times m}, B_k^{[i,j]} \in \mathbb{C}^{N \times n}, C_k^{[i,j]} \in \mathbb{C}^{P \times p}$ and core tensor $\mathcal{G}_k^{[i,j]} \in \mathbb{C}^{m \times n \times p}$ by solving the following problem

$$\begin{aligned} & \min_{A_k^{[i,j]}, B_k^{[i,j]}, C_k^{[i,j]}, \mathcal{G}_k^{[i,j]}} \left\| \mathcal{X}_k^{[i,j]} - \mathcal{G}_k^{[i,j]} \times_1 A_k^{[i,j]} \times_2 B_k^{[i,j]} \times_3 C_k^{[i,j]} \right\|_F^2 \\ & \text{s.t. } (A_k^{[i,j]})^* A_k^{[i,j]} = I_m, (B_k^{[i,j]})^* B_k^{[i,j]} = I_n, (C_k^{[i,j]})^* C_k^{[i,j]} = I_p \end{aligned} \quad (3.2)$$

In the individually Tucker decomposition model (3.2), the mode-1,2 factor matrices $\mathbf{A}_k^{[i,j]}, \mathbf{B}_k^{[i,j]}$ for different channels are distinct and, therefore, cannot be eliminated during SINR calculation. To address this, an straightforward approach is to make the mode-1,2 factor matrices of different channels are identical. For instance, in the case of channel matrix $\mathbf{H}_k^{[i,j]}$ between user- $[i,j]$ and base- k , the compressed channel matrix can be structured in the following manner:

$$\mathbf{H}_k^{[i,j]} \approx \mathbf{A} \tilde{\mathbf{H}}_k^{[i,j]} \mathbf{B}^*, \text{ with } \mathbf{A}^* \mathbf{A} = \mathbf{I}_m, \mathbf{B}^* \mathbf{B} = \mathbf{I}_n. \quad (3.3)$$

With the utilization of this factorization form, the received signal can be conveniently reformulated. As an example, let's consider the term $\mathbf{H}_k^{[i,j]} \mathbf{P}^{[k,l]} \mathbf{x}^{[k,l]}$ in (2.1), with the SVD precoding method $\mathbf{P}^{[k,l]} = \mathbf{V}^{[k,l]}$.

$$\mathbf{H}_k^{[i,j]} \mathbf{P}^{[k,l]} \mathbf{x}^{[k,l]} \approx \mathbf{A} \tilde{\mathbf{H}}_k^{[i,j]} \mathbf{B}^* \mathbf{V}^{[k,l]} \mathbf{x}^{[k,l]} = \mathbf{A} \tilde{\mathbf{H}}_k^{[i,j]} \tilde{\mathbf{V}}^{[k,l]} \mathbf{x}^{[k,l]} \quad (3.4)$$

In this context, the precoding matrix is expressed as $\mathbf{V}^{[k,l]} = \mathbf{B} \tilde{\mathbf{V}}^{[k,l]}$, where $\tilde{\mathbf{V}}^{[k,l]}$ represents the principal left singular vector matrix of $\tilde{\mathbf{H}}_k^{[i,j]}$. Therefore, the factor matrix \mathbf{B} can be eliminated during the precoding process. Similarly, the factor matrix \mathbf{A} can be eliminated during equalization. As a result, SINR computation exclusively involves the compressed and reduced-scale matrix $\tilde{\mathbf{H}}_k^{[i,j]}$. This factorization form significantly accelerates the SINR calculation process.

- **Shared Tucker compression.** Similar to (3.2), one can solve the following optimization problem to obtain the compressed channel tensors

$$\begin{aligned} \min_{\mathbf{A}, \mathbf{B}, \{\mathbf{C}_k^{[i,j]}\}, \{\mathcal{G}_k^{[i,j]}\}} \sum_{[i,j]} \sum_k \left\| \mathcal{X}_k^{[i,j]} - \mathcal{G}_k^{[i,j]} \times_1 \mathbf{A} \times_2 \mathbf{B} \times_3 \mathbf{C}_k^{[i,j]} \right\|_F^2, \\ \text{s.t. } \mathbf{A}^* \mathbf{A} = \mathbf{I}_m, \mathbf{B}^* \mathbf{B} = \mathbf{I}_n, \mathbf{C}_k^{[i,j]*} \mathbf{C}_k^{[i,j]} = \mathbf{I}_p, \text{ for all } i, j, k. \end{aligned} \quad (3.5)$$

Nonetheless, as the number of BSs and UEs increases, achieving a suitably minimized approximation error in (3.5) becomes challenging due to the shared mode-1 and mode-2 factor matrices \mathbf{A} and \mathbf{B} . Consequently, attaining a sufficiently accurate compressed solution becomes difficult.

3.2 Groupwise-Tucker Compression Model

For the above two models can not achieve a good data compression and computation acceleration within an acceptable error rate, we consider a groupwise Tucker compression method. For a given channel matrix $\mathbf{H}_k^{[i,j]}$ between user $[i,j]$ and base station k , the matrix factorization is expressed in the following form:

$$\mathbf{H}_k^{[i,j]} \approx \mathbf{A}_{[i,j]} \tilde{\mathbf{H}}_k^{[i,j]} \mathbf{B}_k^*, \text{ with } \mathbf{A}_{[i,j]}^* \mathbf{A}_{[i,j]} = \mathbf{I}_m, \mathbf{B}_k^* \mathbf{B}_k = \mathbf{I}_n, \quad (3.6)$$

In (3.6) and Figure 2, it can be observed that the left factor matrix $A_{[i,j]}$ represents the factor matrix for the serving and interference channels of user $[i,j]$, while the right factor matrix B_k corresponds to the factor matrix for all channels from base station k . Compared to the factorization form in (3.3), this factorization form incorporates more mode-1,2 factor matrices, resulting in reduced approximation errors. In Section 3.3, we will demonstrate that this relaxation still preserves the property of eliminating the factor matrices $A_{[i,j]}$ and B_k during SINR calculations.

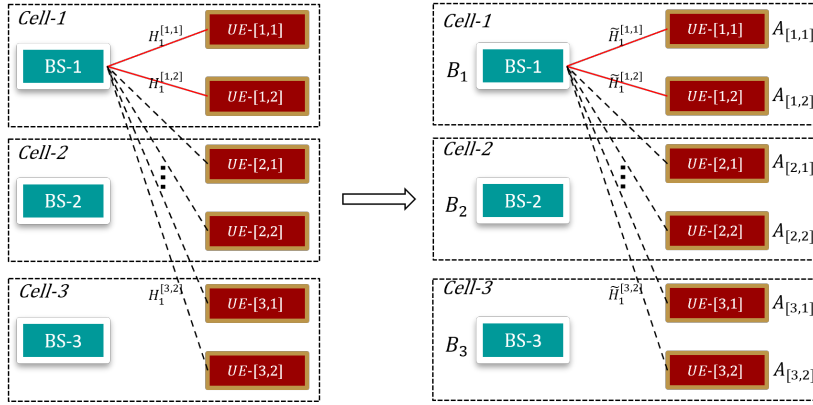


Figure 2: Channel matrices of MIMO system with 3 bases and 2 users per cell before and after compression. The serving channel matrices between BS-1 and UE-[1,1] and UE-[1,2] are represented by two red lines, while the interference channel matrices from BS-1 and UEs in other cells are represented by black dashed lines.

Denote the channel tensor between user- $[i,j]$ and base- k as $\mathcal{X}_k^{[i,j]}$, and its coefficient vector in (2.2) as $\mathbf{c}_k^{[i,j]}$, then the Groupwise Tucker compression model factorizes $\mathcal{X}_k^{[i,j]}$ in the following form

$$\mathcal{X}_k^{[i,j]} \approx \mathcal{G}_k^{[i,j]} \times_1 A_{[i,j]} \times_2 B_k \times_3 C_k^{[i,j]} \quad (3.7)$$

with $A_{[i,j]}^* A_{[i,j]} = I_m, B_k^* B_k = I_n, C_k^{[i,j]*} C_k^{[i,j]} = I_p.$

Plug the (3.7) into (3.1) yields

$$\mathbf{H}_k^{[i,j]} = \mathcal{X}_k^{[i,j]} \times_3 \mathbf{c}_k^{[i,j]*} \approx A_{[i,j]} (\mathcal{G}_k^{[i,j]} \times_3 (\mathbf{c}_k^{[i,j]*} C_k^{[i,j]})) B_k^*. \quad (3.8)$$

The compressed channel matrix in (3.6) can be represented as $\tilde{\mathbf{H}}_k^{[i,j]} = \mathcal{G}_k^{[i,j]} \times_3 (\mathbf{c}_k^{[i,j]*} C_k^{[i,j]})$. Comparing this with (3.1), it appears that an additional matrix-vector multiplication is required to obtain the compressed channel matrix. However, since both $\mathcal{G}_k^{[i,j]}$ and $C_k^{[i,j]}$ are compressed, the overall computational cost is lower than the tensor-vector multiplication in (3.1).

To get the factor matrices and corresponding core tensor, analogous to Tucker decomposition, we define $f_k^{[i,j]} := \left\| \boldsymbol{\mathcal{X}}_k^{[i,j]} - \boldsymbol{\mathcal{G}}_k^{[i,j]} \times_1 \mathbf{A}_{[i,j]} \times_2 \mathbf{B}_k \times_3 \mathbf{C}_k^{[i,j]} \right\|_F^2$ as the approximation error of channel tensor $\boldsymbol{\mathcal{X}}_k^{[i,j]}$ and consider the following model:

$$\begin{aligned} \min f &:= \sum_{[i,j]} \sum_k f_k^{[i,j]} = \sum_{[i,j]} \sum_k \left\| \boldsymbol{\mathcal{X}}_k^{[i,j]} - \boldsymbol{\mathcal{G}}_k^{[i,j]} \times_1 \mathbf{A}_{[i,j]} \times_2 \mathbf{B}_k \times_3 \mathbf{C}_k^{[i,j]} \right\|_F^2, \\ \text{s.t. } &\mathbf{A}_{[i,j]}^* \mathbf{A}_{[i,j]} = \mathbf{I}_m, \mathbf{B}_k^* \mathbf{B}_k = \mathbf{I}_n, \mathbf{C}_k^{[i,j]*} \mathbf{C}_k^{[i,j]} = \mathbf{I}_p, \text{ for all } i, j, k. \end{aligned} \quad (3.9)$$

As analyzed in [33], when minimizing such an objective with orthogonal constraints on the factor matrices, it is more efficient to transform this problem into an equivalent maximization problem. It is easy to verify that if the factor matrices $\mathbf{A}_{[i,j]}, \mathbf{B}_k, \mathbf{C}_k^{[i,j]}$ are fixed, then the optimal $\boldsymbol{\mathcal{G}}_k^{[i,j]}$ is:

$$\boldsymbol{\mathcal{G}}_k^{[i,j]} = \boldsymbol{\mathcal{X}}_k^{[i,j]} \times_1 \mathbf{A}_{[i,j]}^* \times_2 \mathbf{B}_k^* \times_3 \mathbf{C}_k^{[i,j]*}. \quad (3.10)$$

By substituting $\boldsymbol{\mathcal{G}}_k^{[i,j]}$ in (3.10) into $f_k^{[i,j]}$, one gets

$$\begin{aligned} f_k^{[i,j]} &= \left\| \boldsymbol{\mathcal{X}}_k^{[i,j]} \right\|_F^2 - \left\| \boldsymbol{\mathcal{X}}_k^{[i,j]} \times_1 \mathbf{A}_{[i,j]}^* \times_2 \mathbf{B}_k^* \times_3 \mathbf{C}_k^{[i,j]*} \right\|_F^2 \\ &:= \left\| \boldsymbol{\mathcal{X}}_k^{[i,j]} \right\|_F^2 - g_k^{[i,j]} \end{aligned} \quad (3.11)$$

Thus, (3.9) is equivalent to the following maximization problem:

$$\begin{aligned} \max g &:= \sum_{[i,j]} \sum_k g_k^{[i,j]} = \sum_{[i,j]} \sum_k \left\| \boldsymbol{\mathcal{X}}_k^{[i,j]} \times_1 \mathbf{A}_{[i,j]}^* \times_2 \mathbf{B}_k^* \times_3 \mathbf{C}_k^{[i,j]*} \right\|_F^2 \\ \text{s.t. } &\mathbf{A}_{[i,j]}^* \mathbf{A}_{[i,j]} = \mathbf{I}_m, \mathbf{B}_k^* \mathbf{B}_k = \mathbf{I}_n, \mathbf{C}_k^{[i,j]*} \mathbf{C}_k^{[i,j]} = \mathbf{I}_p, \text{ for all } i, j, k. \end{aligned} \quad (3.12)$$

For solving (3.12), similar to Algorithm 1, one can first use the singular vectors of matricization of $\boldsymbol{\mathcal{X}}_k^{[i,j]}$ in different mode as the initialization of $\mathbf{A}_{[i,j]}, \mathbf{B}_k$ and $\mathbf{C}_k^{[i,j]}$, respectively. Then update $\mathbf{A}_{[i,j]}, \mathbf{B}_k$ and $\mathbf{C}_k^{[i,j]}$ alternatively with the optimal solution of corresponding subproblem, e.g.,

- For $\mathbf{A}_{[i,j]}$

$$\begin{aligned} \mathbf{A}_{[i,j]} &= \operatorname{argmax}_{\mathbf{A}^* \mathbf{A} = \mathbf{I}_m} \sum_k g_k^{[i,j]} \left(\mathbf{A}, \mathbf{B}_k, \mathbf{C}_k^{[i,j]} \right) \\ &= m \text{ principal eigenvectors of } \sum_k \left({}_1 \mathbf{M}_k^{[i,j]} {}_1 \mathbf{M}_k^{[i,j]*} \right) \end{aligned} \quad (3.13)$$

where ${}_1 \mathbf{M}_k^{[i,j]} = \left(\boldsymbol{\mathcal{X}}_k^{[i,j]} \times_2 \mathbf{B}_k^* \times_3 \mathbf{C}_k^{[i,j]*} \right)_{(1)}$.

- For \mathbf{B}_k

$$\begin{aligned} \mathbf{B}_k &= \operatorname{argmax}_{\mathbf{B}^* \mathbf{B} = \mathbf{I}_n} \sum_{[i,j]} g_k^{[i,j]} \left(\mathbf{A}_{[i,j]}, \mathbf{B}, \mathbf{C}_k^{[i,j]} \right) \\ &= n \text{ principle eigenvectors of } \sum_{[i,j]} \left({}_2\mathbf{M}_k^{[i,j]} {}_2\mathbf{M}_k^{[i,j]*} \right) \end{aligned} \quad (3.14)$$

$$\text{where } {}_2\mathbf{M}_k^{[i,j]} = \left(\mathcal{X}_k^{[i,j]} \times_1 \mathbf{A}_{[i,j]}^* \times_3 \mathbf{C}_k^{[i,j]*} \right)_{(2)}.$$

- For $\mathbf{C}_k^{[i,j]}$

$$\begin{aligned} \mathbf{C}_k^{[i,j]} &= \operatorname{argmax}_{\mathbf{C}^* \mathbf{C} = \mathbf{I}_p} g_k^{[i,j]} \left(\mathbf{A}_{[i,j]}, \mathbf{B}_k, \mathbf{C} \right) \\ &= p \text{ principle eigenvectors of } {}_3\mathbf{M}_k^{[i,j]} {}_3\mathbf{M}_k^{[i,j]*} \end{aligned} \quad (3.15)$$

$$\text{where } {}_3\mathbf{M}_k^{[i,j]} = \left(\mathcal{X}_k^{[i,j]} \times_1 \mathbf{A}_{[i,j]}^* \times_2 \mathbf{B}_k^* \right)_{(3)}.$$

Details of updates are summarized in Algorithm2.

Algorithm 2 Groupwise Tucker compression algorithm

```

1: Initialize  $(\mathbf{A}_{[i,j]})_0, (\mathbf{B}_k)_0$  and  $(\mathbf{C}_k^{[i,j]})_0$  for  $[i,j] \in [J] \times [K_i]$  and  $k \in [J]$ .
2: for  $s=0, \dots, S-1$  do
3:   for  $[i,j] \in [J] \times [K_i]$  do
4:     Compute  $(\mathbf{A}_{[i,j]})_{s+1}$  through (3.13) with  $(\mathbf{B}_k)_s$  and  $(\mathbf{C}_k^{[i,j]})_s$ , for  $k \in [J]$ .
5:   end for
6:   for  $k \in [J]$  do
7:     Compute  $(\mathbf{B}_k)_{s+1}$  through (3.14) with  $(\mathbf{A}_{[i,j]})_{s+1}$  and  $(\mathbf{C}_k^{[i,j]})_s$ , for  $[i,j] \in [J] \times [K_i]$ 
8:   end for
9:   for  $(k, [i,j]) \in [J] \times [J] \times [K_i]$  do
10:    Compute  $(\mathbf{C}_k^{[i,j]})_{s+1}$  through (3.15) with  $(\mathbf{A}_{[i,j]})_{s+1}$  and  $(\mathbf{B}_k)_{s+1}$ .
11:   end for
12: end for
13: for  $(k, [i,j]) \in [J] \times [J] \times [K_i]$  do
14:    $(\mathcal{G}_k^{[i,j]})_S = \mathcal{X}_k^{[i,j]} \times_1 (\mathbf{A}_{[i,j]})_S^* \times_2 (\mathbf{B}_k)_S^* \times_3 (\mathbf{C}_k^{[i,j]})_S^*$ .
15: end for
Output:  $(\mathbf{A}_{[i,j]})_S, (\mathbf{B}_k)_S, (\mathbf{C}_k^{[i,j]})_S$  and  $(\mathcal{G}_k^{[i,j]})_S$  for  $[i,j] \in [J] \times [K_i]$  and  $k \in [J]$ .

```

In Algorithm 2, it follows a Gauss-Seidel methodology that the factor matrices $\mathbf{A}_{[i,j]}, \mathbf{B}_k$ and $\mathbf{C}_k^{[i,j]}$ are alternately updated. The computation of the core tensors $\mathcal{G}_k^{[i,j]}$ is not required in each iteration but is performed once after completion. The algorithm will converge to a solution where the objective function f ceases to decrease. However, similar

to the HOOI algorithm [35], this method is not guaranteed to converge to the global optimum. Usually, one can use a predefined iteration number S as a stopping criterion.

3.3 Storage and SINR Complexity Reduction

For ease of exposition, we assume the numbers of users in all BSs are equal, denoted as K . Then with J BSs there are J^2K channels in the entire system. So before compression, it is necessary to store J^2K complete channel tensors, each with a size of $M \times N \times P$. After compression using (3.9), there are JK first-mode factor matrices $\mathbf{A}_{[i,j]}$ with dimensions $M \times m$, J second-mode factor matrices \mathbf{B}_k with dimensions $N \times n$, J^2K third-mode factor matrices $\mathbf{C}_k^{[i,j]}$ with dimensions $P \times p$ and core tensors $\mathcal{G}_k^{[i,j]}$ with size of $m \times n \times p$. Table 1 outlines the storage requirements before and after compression.

	Original	Compressed
Storage	J^2KMNP	$J^2K(mnp + Pp) + JKMm + JNn$

Table 1: The storage (measured in complex double-precision floating-point numbers) of whole system before and after compression.

For the SINR calculation, the first step is to reconstruct the channel matrices from channel tensors. Then is to compute the precoding matrix $\mathbf{P}^{[i,j]}$, covariance matrix $\mathbf{Q}^{[i,j]}$ and its inversion, along with the filter matrix $\mathbf{W}^{[i,j]}$. The SINR is finally determined using (2.5). The comparative computational complexity for each step before and after compression is outlined below.

- For reconstructing channel matrices $\mathbf{H}_k^{[i,j]} / \tilde{\mathbf{H}}_k^{[i,j]}$. According to (3.8), before compression, directly performing a tensor-vector product $\mathcal{X}_k^{[i,j]} \times_3 \mathbf{c}_k^{[i,j]*}$ requires MNP floating-point operations (flops). After compression, $(\mathcal{G}_k^{[i,j]} \times_3 (\mathbf{c}_k^{[i,j]*} \mathbf{C}_k^{[i,j]}))$ involves a matrix-vector product and a tensor-vector product, requiring $mnp + Pp$ flops.
- For the precoding matrix $\mathbf{V}^{[k,l]} / \tilde{\mathbf{V}}^{[k,l]}$. Before compression, directly computing truncated- L SVD of channel matrix $\mathbf{H}_k^{[k,l]}$ requires $O(MNL)$ flops. After compression, only the truncated- L SVD of $\tilde{\mathbf{H}}_k^{[k,l]}$ is needed due to the orthogonality of $\mathbf{A}_{[k,l]}$ and \mathbf{B}_k . It requires $O(mnL)$ flops to obtain $\tilde{\mathbf{V}}^{[k,l]}$, and the relationship between $\mathbf{V}^{[k,l]}$ and $\tilde{\mathbf{V}}^{[k,l]}$ is:

$$\mathbf{V}^{[k,l]} \approx \mathbf{B}_k \tilde{\mathbf{V}}^{[k,l]}, \quad (3.16)$$

thereby eliminating the right factor matrix \mathbf{B}_k in precoding process:

$$\mathbf{H}_k^{[i,j]} \mathbf{V}^{[k,l]} \approx \mathbf{A}_{[i,j]} \tilde{\mathbf{H}}_k^{[i,j]} \tilde{\mathbf{V}}^{[k,l]} \quad (3.17)$$

- For the covariance matrix $\mathbf{Q}^{[i,j]} / \tilde{\mathbf{Q}}^{[i,j]}$ and its inversion. Plug (3.17) into (2.4),

$$\begin{aligned} \mathbf{Q}^{[i,j]} &= \sum_{k=1}^J \sum_{l=1}^K \mathbf{H}_k^{[i,j]} \mathbf{V}^{[k,l]} (\mathbf{H}_k^{[i,j]} \mathbf{V}^{[k,l]})^* + \sigma^2 \mathbf{I}_M \\ &\approx \mathbf{A}_{[i,j]} \left(\sum_{k=1}^J \sum_{l=1}^K \tilde{\mathbf{H}}_k^{[i,j]} \tilde{\mathbf{V}}^{[k,l]} (\tilde{\mathbf{H}}_k^{[i,j]} \tilde{\mathbf{V}}^{[k,l]})^* \right) \mathbf{A}_{[i,j]}^* + \sigma^2 \mathbf{I}_M, \end{aligned} \quad (3.18)$$

Apply Woodbury formula [36] to the last equation of (3.18), the inversion $(\mathbf{Q}^{[i,j]})^{-1}$ is given by

$$(\mathbf{Q}^{[i,j]})^{-1} \approx \frac{1}{\sigma^2} \mathbf{I}_M - \frac{1}{\sigma^2} \mathbf{A}_{[i,j]} (\tilde{\mathbf{Q}}^{[i,j]})^{-1} (\tilde{\mathbf{Q}}^{[i,j]} - \sigma^2 \mathbf{I}_m) \mathbf{A}_{[i,j]}^*, \quad (3.19)$$

where

$$\tilde{\mathbf{Q}}^{[i,j]} = \sum_{k=1}^J \sum_{l=1}^K \tilde{\mathbf{H}}_k^{[i,j]} \tilde{\mathbf{V}}^{[k,l]} (\tilde{\mathbf{H}}_k^{[i,j]} \tilde{\mathbf{V}}^{[k,l]})^* + \sigma^2 \mathbf{I}_m.$$

here the inversion of the $\mathbf{Q}^{[i,j]}$ is substituted with the inversion of a smaller matrix $\tilde{\mathbf{Q}}^{[i,j]}$ and several matrix-matrix multiplications. The matrix $\mathbf{A}_{[i,j]}$ does not need to be explicitly multiplied as it can be eliminated in subsequent computations owing to its orthogonality.

In (3.18), the matrix-matrix product $\mathbf{H}_k^{[i,j]} \mathbf{V}^{[k,l]}$ and $\tilde{\mathbf{H}}_k^{[i,j]} \tilde{\mathbf{V}}^{[k,l]}$ requires MNL flops and mnL flops, respectively. Then $\mathbf{H}_k^{[i,j]} \mathbf{V}^{[k,l]} (\mathbf{H}_k^{[i,j]} \mathbf{V}^{[k,l]})^*$ and $\tilde{\mathbf{H}}_k^{[i,j]} \tilde{\mathbf{V}}^{[k,l]} (\tilde{\mathbf{H}}_k^{[i,j]} \tilde{\mathbf{V}}^{[k,l]})^*$ requires M^2L flops and m^2L flops, respectively. Consequently, calculating $\mathbf{Q}^{[i,j]}$ and $\tilde{\mathbf{Q}}^{[i,j]}$ requires $JK(MNL + M^2L)$ and $JK(mnL + m^2L)$ flops, respectively. $(\mathbf{Q}^{[i,j]})^{-1}$ and $(\tilde{\mathbf{Q}}^{[i,j]})^{-1}$ requires $O(M^3)$ and $O(m^3)$ flops, respectively. The matrix-matrix multiplications $(\tilde{\mathbf{Q}}^{[i,j]})^{-1} (\tilde{\mathbf{Q}}^{[i,j]} - \sigma^2 \mathbf{I}_m)$ requires m^3 flops.

- For the filter matrix $\mathbf{W}^{[i,j]} / \tilde{\mathbf{W}}^{[i,j]}$. By substituting (3.19) into (2.3), $\mathbf{W}^{[i,j]}$ can be expressed as:

$$\mathbf{W}^{[i,j]} \approx \mathbf{A}_{[i,j]} \tilde{\mathbf{W}}^{[i,j]}, \quad (3.20)$$

where $\tilde{\mathbf{W}}^{[i,j]} = \frac{1}{\sigma^2} (\mathbf{I}_m - (\tilde{\mathbf{Q}}^{[i,j]})^{-1} (\tilde{\mathbf{Q}}^{[i,j]} - \sigma^2 \mathbf{I}_m)) \tilde{\mathbf{H}}_i^{[i,j]} \tilde{\mathbf{V}}^{[i,j]}$. In this procedure, the matrix is still retained $\mathbf{A}_{[i,j]}$ and not explicitly multiplied. The matrix $(\tilde{\mathbf{Q}}^{[i,j]})^{-1} (\tilde{\mathbf{Q}}^{[i,j]} - \sigma^2 \mathbf{I}_m)$ and $\tilde{\mathbf{H}}_i^{[i,j]} \tilde{\mathbf{V}}^{[i,j]}$ have already been obtained in the previous procedure. Consequently, the computational complexity for $\mathbf{W}^{[i,j]}$ and $\tilde{\mathbf{W}}^{[i,j]}$ is M^2L and $m^2L + mL$ flops, respectively.

- For $\mathbf{s}_r^{[i,j]} / \tilde{\mathbf{s}}_r^{[i,j]}$ and $\widetilde{\text{SINR}}_r^{[i,j]} / \widetilde{\text{SINR}}_r^{[i,j]}$. We can finally eliminate the factor matrix $\mathbf{A}_{[i,j]}$. The $\mathbf{s}_r^{[i,j]}$ in (2.5) only involves a vector inner product, thus it requires M flops

while for $\tilde{\mathbf{s}}_r^{[i,j]}$,

$$\begin{aligned}\tilde{\mathbf{s}}_r^{[i,j]} &= \left| \left[\widetilde{\mathbf{W}}^{[i,j]} \right]_r^* \mathbf{A}_{[i,j]}^* \mathbf{A}_{[i,j]} \left[\widetilde{\mathbf{H}}_i^{[i,j]} \widetilde{\mathbf{V}}^{[i,j]} \right]_r \right|^2 \\ &= \left| \left[\widetilde{\mathbf{W}}^{[i,j]} \right]_r^* \left[\widetilde{\mathbf{H}}_i^{[i,j]} \widetilde{\mathbf{V}}^{[i,j]} \right]_r \right|^2\end{aligned}\quad (3.21)$$

it requires m flops. For $\text{SINR}_r^{[i,j]}$, the $\left[\mathbf{W}^{[i,j]} \right]_r^* \mathbf{Q}^{[i,j]} \left[\mathbf{W}^{[i,j]} \right]_r$ in (2.5) needs a matrix-vector product and a vector-vector product, which needs $M^2 + M$ flops. Similarly, $\widetilde{\text{SINR}}_r^{[i,j]}$ needs $m^2 + m$ flops.

Clearly, the SINR calculation in (2.5) can be directly evaluated using the compressed channel matrix $\widetilde{\mathbf{H}}_k^{[i,j]}$. A comparison of the total computational complexity for SINR using complete and compressed channel matrices is presented in Figure 3.

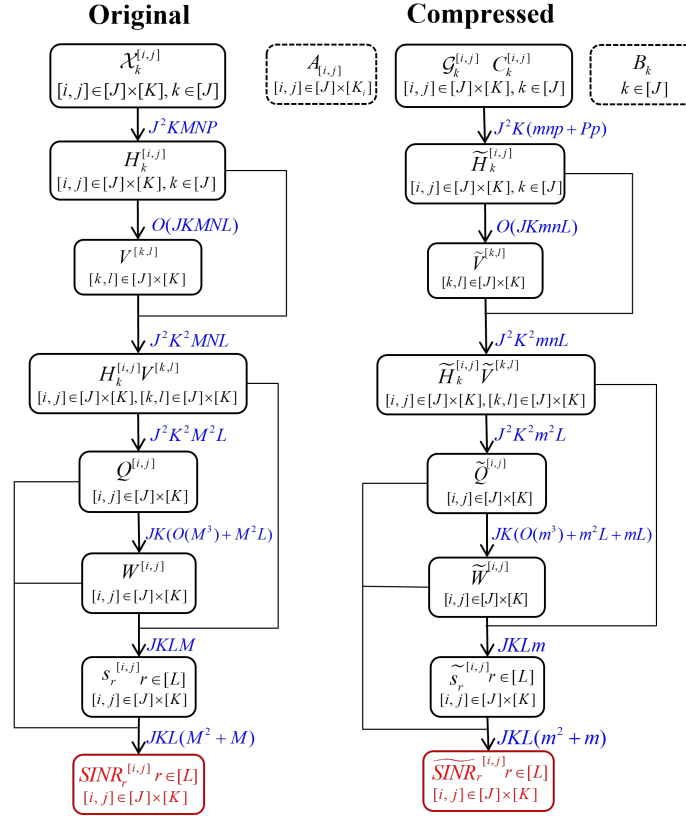


Figure 3: Computational complexity comparison.

Indeed, utilizing the compressed channel matrix $\widetilde{\mathbf{H}}_k^{[i,j]}$ with a smaller size leads to a reduction in computational complexity. However, this decrease in size comes at the cost

of increased approximation error. Consequently, choosing the compressed channel size necessitates careful consideration to strike an optimal balance between computational efficiency and accuracy. The subsequent section will delve into this trade-off through a series of experiments.

4 Numerical Experiments

In this section, we conduct experiments on MIMO systems of different scales and channels to evaluate the numerical performance of the proposed compression models. The channel matrices used in the experiments are generated based on the specifications provided by the 3rd Generation Partnership Project (3GPP) [23] at a fixed time point. We consider two popular channel matrix sizes: 64×512 (64 receiving and 512 transmitting antennas) and 8×256 , the submatrices number P is 401. Figure 4 provides a pictorial depiction of a MIMO system comprising 21 base stations and 10 users per cell used in our experiments. In the experiments, we simplify the scenario by considering only the inter-cell interference from the first user equipment (UE) of other cells and ignoring the intra-cell interference.

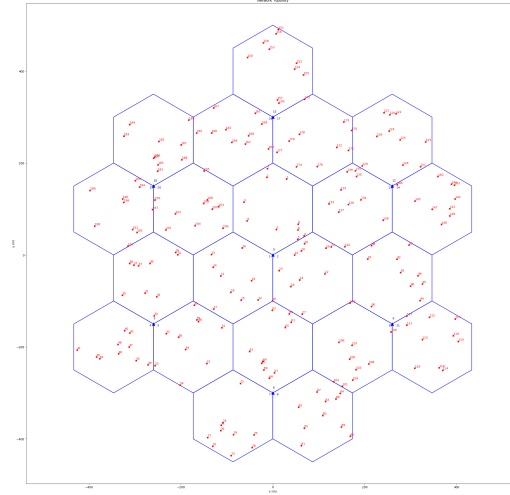


Figure 4: Topological diagram for 21 BSs and 210 UEs MIMO system.

To evaluate the performance of the compression models in terms of reducing storage requirements and accelerating SINR computation, we introduce two compression ratios: R_s and R_t . The compression ratio R_s is defined as the ratio of memory usage for channel data before and after compression (as shown in Table 1). R_s can be directly calculated by the following equation.

$$R_s = \frac{J^2 K M N P}{J^2 K (m n p + P p) + J K M m + J N n} \quad (4.1)$$

For the speedup ratio R_t , we count the run time of calculating SINR as depicted in Figure 3. Assume t_1 and t_2 are the run time for original channel data and compressed data, respectively, then $R_t = t_1/t_2$.

We evaluate the accuracy of the compression models by calculating the mean relative error e_c of the SINR values before and after compression. The mean relative error is computed as the average of the absolute differences between the original SINR values $s_r^{[i,j]}$ and the compressed SINR values $\widetilde{s}_r^{[i,j]}$ for all $r \in [L], [i,j] \in [J] \times [K]$, divided by the original SINR values, e.g.,

$$e_c = \text{mean of } \left\{ \left| \frac{\text{SINR}_r^{[i,j]} - \widetilde{\text{SINR}}_r^{[i,j]}}{\text{SINR}_r^{[i,j]}} \right| \right\}. \quad (4.2)$$

From Tables 1 and Figure 3, we can observe a strong correlation between R_t and R_s . Smaller compressed channel sizes lead to higher R_s and R_t but lower accuracy due to increased approximation errors. In our experiments, we compare three compression models: Individual Tucker model in (3.2), Shared Tucker model in (3.5) and Groupwise Tucker model in (3.9). We firstly maintain the mean relative error e_c at around 10% and adjust the compression parameters m, n, p to achieve higher values of R_s and R_t in the Groupwise Tucker model. Since M is already small, we focus on tuning the parameters n and p while setting m to be equal (or close) to M . Subsequently, we set the same compression parameters m, n, p in the Individual Tucker model and Shared Tucker model. The results of three compression models are summarized in Table 2.

		Settings			Results		
L	(M, N, P)	K	(m, n, p)	Model	R_t	R_s	e_c
21	(64,512,401)	5	(60,230,150)	Individual Tucker	0.17951	5.8354	5.6042%
				Shared Tucker	5.7931	6.1684	12.5947%
				Groupwise Tucker	6.1904	6.1648	9.3929%
		10	(60,270,190)	Individual Tucker	0.17072	3.9863	2.9760%
				Shared Tucker	3.3805	4.1658	13.2991%
				Groupwise Tucker	4.1080	4.1648	8.2277%
21	(8,256,401)	5	(8,130,120)	Individual Tucker	0.15937	3.9815	6.5190%
				Shared Tucker	1.2023	4.7489	13.3681%
				Groupwise Tucker	1.3500	4.7405	10.8535%
		10	(8,140,140)	Individual Tucker	0.14927	3.3003	3.9147%
				Shared Tucker	1.1768	3.8566	9.9698%
				Groupwise Tucker	1.1014	3.8536	9.0037%

Table 2: Compression results of Groupwise Tucker, Individual Tucker and Shared Tucker models for MIMO systems with different scales and channels.

In rows 3, 6 (or rows 9, 12) of Table 2, we fix M, N, P and consider three different

numbers of UEs K in each BS. We tune m, n, p such that the relative error e_c is below 10%. The results indicate that larger compression sizes m, n, p (resulting in smaller R_t and R_s) are required to ensure the relative error e_c when more users are considered.

In rows 1-3 (or rows 4-6, rows 7-9, rows 10-12) of Table 2, we compare the three compression models under the same settings. The error of the Individual Tucker decomposition is smaller than that of the Groupwise Tucker model and Shared Tucker model, but the speedup ratio R_t of the Individual Tucker decomposition is less than 1, indicating that it requires more computational cost compared to the original data. Comparing the Groupwise Tucker and Shared Tucker models, they have similar performance on accelerating the SINR process with R_t greater than 1, while the solution of Shared Tucker model is more accurate as the relative error e_c is notably smaller than that of the Groupwise Tucker model.

For the compression ratio R_s , the Shared Tucker model has a slightly higher value than the Groupwise Tucker model. This is consistent with their factorization forms in their respective models. Comparing rows 1-6 with rows 7-12 of Table 2 respectively, we can observe that the compression performance is better when the channel size is larger, particularly in terms of the speedup ratio R_t .

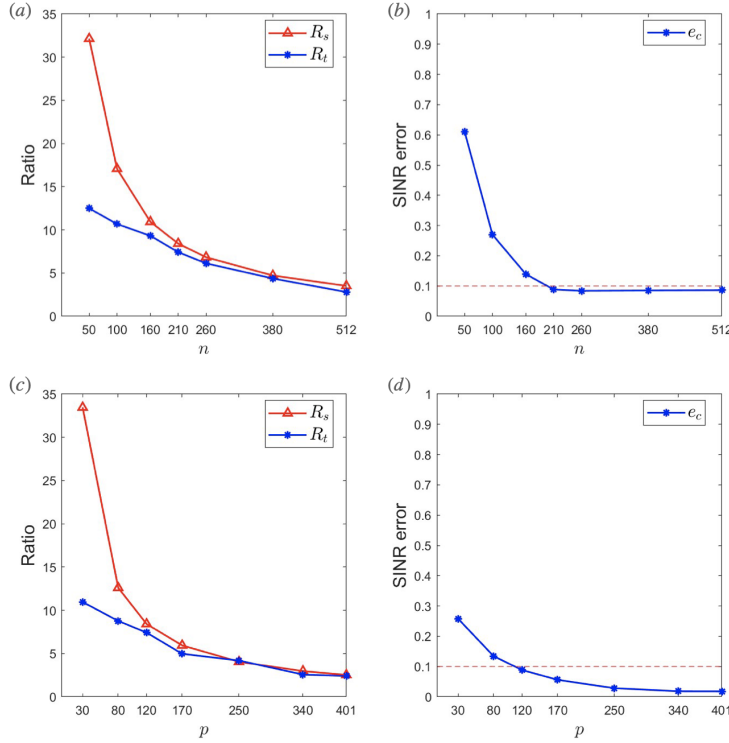


Figure 5: The compression results for channel data with $L=21$, $K=2$ and $(M, N, P) = (64, 512, 401)$. The red dashed lines in Figure (b) and Figure (d) represent the 10% mean relative error we desire.

In addition to the previous results, we also provide the univariate tuning results of Groupwise Tucker compression model to show the impact of changing the number of compressed columns (or submatrices) on the performance metrics. We use the channel data with $L = 21$ and $K = 2$ and the antenna configuration is $(M, N, P) = (64, 512, 401)$. We first fix $(m, p) = (60, 120)$ and vary the compressed columns number n , the result for (R_t, R_c) and e_c are shown in Figure 5(a) and Figure 5(b), respectively. Also we consider to fix (m, n) and vary p , the corresponding results are depicted in Figure 5(c) and Figure 5(d).

Upon inspection of (4.1) derived from the storage complexity in Table 1, we can deduce that R_s is inversely proportional to p and n . The numerical observations depicted in (a) and (c) of Figure 5 align with our theoretical predictions. Regarding the SINR error plots in Figure 5 (b) and (d), it appears that smaller values of n or p are sufficient to achieve the best SINR error performance. This suggests that a lower number of compressed columns or submatrices can effectively preserve the accuracy of the SINR calculation.

5 Conclusion and Discussion

In this paper, we propose the Groupwise Tucker compression model based on Tucker decomposition to compress channel data in massive MIMO systems. Our approach enables faster signal transmission operations, particularly in SINR calculation, while significantly reducing storage requirements. The numerical results demonstrate substantial improvements in both storage efficiency and SINR calculation speed with high precision. However, there are two remaining issues that require further investigation.

Firstly, the current algorithm relies on SVD, which can be time-consuming due to the high dimensions of channel data in our problem. Although the compression task can be performed offline, reducing this computational cost is worth pondering. One possible solution is to incorporate SVD-free techniques into the framework, as suggested in a recent paper [37].

Secondly, the selection of compression parameters currently involves a time-consuming trial-and-error approach. While we have explored using evolutionary algorithms such as Particle Swarm Optimization (PSO) [38] and surrogate learning to address this issue, none of these methods have yielded satisfactory results. Therefore, another avenue for improvement is to develop rank-selection approaches for determining compression parameters more efficiently.

Addressing these two issues would further enhance the practicality and efficiency of the Groupwise Tucker compression model, making it more viable for real-world applications.

References

- [1] Helmut Bolcskei. Mimo-ofdm wireless systems: basics, perspectives, and challenges. *IEEE wireless communications*, 13(4):31–37, 2006.
- [2] Michael A Jensen and Jon W Wallace. A review of antennas and propagation for mimo wireless communications. *IEEE Transactions on Antennas and Propagation*, 52(11):2810–2824, 2004.
- [3] Bruno Clerckx and Claude Oestges. *MIMO wireless networks: channels, techniques and standards for multi-antenna, multi-user and multi-cell systems*. Academic Press, 2013.
- [4] Lavish Kansal, Vishal Sharma, and Jagjit Singh. Multiuser massive mimo-ofdm system incorporated with diverse transformation for 5g applications. *Wireless Personal Communications*, 109(4):2741–2756, 2019.
- [5] KNR Surya Vara Prasad, Ekram Hossain, and Vijay K Bhargava. Energy efficiency in massive mimo-based 5g networks: Opportunities and challenges. *IEEE Wireless Communications*, 24(3):86–94, 2017.
- [6] Thomas L Marzetta. Massive mimo: an introduction. *Bell Labs Technical Journal*, 20:11–22, 2015.
- [7] Erik G Larsson, Ove Edfors, Fredrik Tufvesson, and Thomas L Marzetta. Massive mimo for next generation wireless systems. *IEEE communications magazine*, 52(2):186–195, 2014.
- [8] Robin Chataut and Robert Akl. Massive mimo systems for 5g and beyond networks—overview, recent trends, challenges, and future research direction. *Sensors*, 20(10):2753, 2020.
- [9] Thomas L Marzetta. Noncooperative cellular wireless with unlimited numbers of base station antennas. *IEEE transactions on wireless communications*, 9(11):3590–3600, 2010.
- [10] David Tse and Pramod Viswanath. *Fundamentals of wireless communication*. Cambridge university press, 2005.
- [11] Weiliang Zeng, Chengshan Xiao, Mingxi Wang, and Jianhua Lu. Linear precoding for finite-alphabet inputs over mimo fading channels with statistical csi. *IEEE Transactions on Signal Processing*, 60(6):3134–3148, 2012.
- [12] Narendra Anand, Jeongkeun Lee, Sung-Ju Lee, and Edward W Knightly. Mode and user selection for multi-user mimo wlans without csi. In *2015 IEEE Conference on Computer Communications (INFOCOM)*, pages 451–459. IEEE, 2015.
- [13] Zhenhua Xie, Robert T. Short, and Craig K. Rushforth. A family of suboptimum detectors for coherent multiuser communications. *IEEE journal on selected areas in communications*, 8(4):683–690, 1990.
- [14] Yangxurui Liu, Ove Edfors, Liang Liu, and Viktor Öwall. Reducing on-chip memory for massive mimo baseband processing using channel compression. In *2017 IEEE 86th Vehicular Technology Conference (VTC-Fall)*, pages 1–5. IEEE, 2017.
- [15] Shahram Zarei, Wolfgang Gerstaecker, Ralf R Müller, and Robert Schober. Low-complexity linear precoding for downlink large-scale mimo systems. In *2013 IEEE 24th Annual International Symposium on Personal, Indoor, and Mobile Radio Communications (PIMRC)*, pages 1119–1124. IEEE, 2013.
- [16] Andreas Benzin, Giuseppe Caire, Yonatan Shadmi, and Antonia M Tulino. Low-complexity truncated polynomial expansion dl precoders and ul receivers for massive mimo in correlated channels. *IEEE Transactions on Wireless Communications*, 18(2):1069–1084, 2019.
- [17] Sammaiah Thurpati and P Muthuchidamabaranathan. Performance analysis of linear and hybrid precoding on massive mimo system using truncated polynomial expansion. *Wireless*

- Personal Communications*, 126(2):1129–1144, 2022.
- [18] Michael L Honig and Weimin Xiao. Performance of reduced-rank linear interference suppression. *IEEE Transactions on Information Theory*, 47(5):1928–1946, 2001.
- [19] Yonghee Han, Wonjae Shin, and Jungwoo Lee. Projection based feedback compression for fdd massive mimo systems. In *2014 IEEE Globecom Workshops (GC Wkshps)*, pages 364–369. IEEE, 2014.
- [20] Min Soo Sim, Jeonghun Park, Chan-Byoung Chae, and Robert W Heath. Compressed channel feedback for correlated massive mimo systems. *Journal of Communications and Networks*, 18(1):95–104, 2016.
- [21] Ping-Heng Kuo, HT Kung, and Pang-An Ting. Compressive sensing based channel feedback protocols for spatially-correlated massive antenna arrays. In *2012 IEEE Wireless Communications and Networking Conference (WCNC)*, pages 492–497. IEEE, 2012.
- [22] Byungju Lee, Junil Choi, Ji-Yun Seol, David J Love, and Byonghyo Shim. Antenna grouping based feedback compression for fdd-based massive mimo systems. *IEEE Transactions on Communications*, 63(9):3261–3274, 2015.
- [23] 3GPP. Study on channel model for frequencies from 0.5 to 100 ghz. Technical report (TR) 36.331, 3rd Generation Partnership Project (3GPP), 04 2022. Version 14.2.2.
- [24] J Douglas Carroll and Jih-Jie Chang. Analysis of individual differences in multidimensional scaling via an n-way generalization of “eckart-young” decomposition. *Psychometrika*, 35(3):283–319, 1970.
- [25] Richard A Harshman et al. Foundations of the parafac procedure: Models and conditions for an “ explanatory” multimodal factor analysis. 1970.
- [26] Ledyard R Tucker. Some mathematical notes on three-mode factor analysis. *Psychometrika*, 31(3):279–311, 1966.
- [27] Ian T Jolliffe. *Principal component analysis for special types of data*. Springer, 2002.
- [28] Karl Pearson. Liii. on lines and planes of closest fit to systems of points in space. *The London, Edinburgh, and Dublin philosophical magazine and journal of science*, 2(11):559–572, 1901.
- [29] Ivan V Oseledets. Tensor-train decomposition. *SIAM Journal on Scientific Computing*, 33(5):2295–2317, 2011.
- [30] Yinchong Yang, Denis Krompass, and Volker Tresp. Tensor-train recurrent neural networks for video classification. In *International Conference on Machine Learning*, pages 3891–3900. PMLR, 2017.
- [31] Yi Jiang, Mahesh K Varanasi, and Jian Li. Performance analysis of zf and mmse equalizers for mimo systems: An in-depth study of the high snr regime. *IEEE Transactions on Information Theory*, 57(4):2008–2026, 2011.
- [32] Emre Telatar. Capacity of multi-antenna gaussian channels. *European transactions on telecommunications*, 10(6):585–595, 1999.
- [33] Tamara G Kolda and Brett W Bader. Tensor decompositions and applications. *SIAM review*, 51(3):455–500, 2009.
- [34] Lieven De Lathauwer, Bart De Moor, and Joos Vandewalle. A multilinear singular value decomposition. *SIAM journal on Matrix Analysis and Applications*, 21(4):1253–1278, 2000.
- [35] Lieven De Lathauwer, Bart De Moor, and Joos Vandewalle. On the best rank-1 and rank- (r_1, r_2, \dots, r_n) approximation of higher-order tensors. *SIAM journal on Matrix Analysis and Applications*, 21(4):1324–1342, 2000.
- [36] Elizabeth L Yip. A note on the stability of solving a rank-p modification of a linear system by the sherman–morrison–woodbury formula. *SIAM Journal on Scientific and Statistical Computing*, 7(2):507–513, 1986.

- [37] Chuanfu Xiao, Chao Yang, and Min Li. Efficient alternating least squares algorithms for low multilinear rank approximation of tensors. *Journal of Scientific Computing*, 87:1–25, 2021.
- [38] James Kennedy and Russell Eberhart. Particle swarm optimization. In *Proceedings of ICNN'95-international conference on neural networks*, volume 4, pages 1942–1948. IEEE, 1995.